Journal of Advanced Research 28 (2021) 209–219

Contents lists available at ScienceDirect

Journal of Advanced Research

journal homepage: www.elsevier.com/locate/jare

Early label-free analysis of mitochondrial redox states by Raman spectroscopy predicts septic outcomes

Meiyan Wu, Kairui Pu, Tao Jiang, Qian Zhai, Zhi Ma, Hongli Ma, Fuxing Xu, Zhanqin Zhang *, Qiang Wang *

Department of Anesthesiology & Center for Brain Science, The First Affiliated Hospital of Xi'an Jiaotong University, Xi'an 710061, Shaanxi, China

HIGHLIGHTS

- Resonance Raman spectroscopy was applied to *in vivo* detection of the mitochondrial redox state in septic mice for the first time.
- Monitoring mitochondrial redox states using resonance Raman spectroscopy had higher prognostic accuracy for mortality than the lactate level during sepsis and could be a novel diagnostic marker for predicting septic outcomes at an early time point.
- Resonance Raman spectroscopy could detect mitochondrial dysfunction in sepsis and provide a biomarker that can be a specific target of adjunctive treatment.

GRAPHICAL ABSTRACT

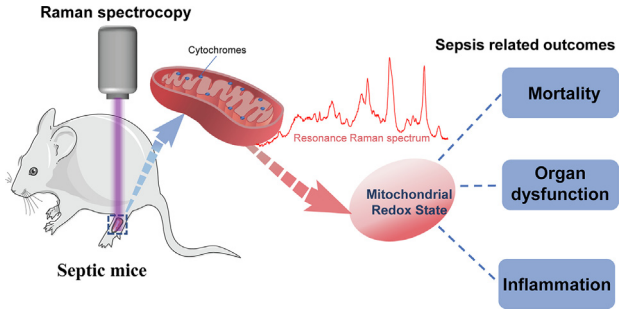

ARTICLE INFO

Article history:
Received 1 April 2020
Revised 10 June 2020
Accepted 29 June 2020
Available online 02 July 2020

Keywords:
Sepsis
Inflammatory response
Multiple organ failure
Mitochondrial redox state
Resonance Raman spectrum
Label-free

ABSTRACT

Background: Sepsis remains an unacceptably high mortality due to the lack of biomarkers for predicting septic outcomes in the early period. Mitochondrial redox states play a pivotal role in this condition and are disturbed early in the development of sepsis. Here, we hypothesized that visualizing mitochondrial redox states via resonance Raman spectroscopy (RRS) could identify septic outcomes at an early time point. Sepsis was induced by cecal ligation and puncture (CLP). We applied RRS analysis at baseline and 30 min, 1 h, 2 h, 4 h, and 6 h after CLP, and the mitochondrial redox states were identified. The levels of blood lactate as a predictor in sepsis were assessed. Our study is the first to reveal the possibility of *in vivo* detection of the mitochondrial redox state by using RRS in septic mice. The peak area for the Raman reduced mitochondrial fraction, the indicator of mitochondrial redox states, fluctuated significantly at 2 h after CLP. This fluctuation occurred earlier than the change in lactate level. Moreover, this fluctuation had higher prognostic accuracy for mortality than the lactate level during sepsis and could be a novel diagnostic marker for predicting septic outcomes according to the cutoff value of 1.059, which had a sensitivity of 80% and a specificity of 90%.
Objectives: To explore an effective indicator concerning mitochondrial redox states in the early stage of sepsis and to predict septic outcomes accurately *in vivo* using non-invasive and label-free Resonance Raman spectroscopy (RRS) analysis.
Methods: Mitochondria, primary skeletal muscle cells and*ex-vivo* muscles harvested from gastrocnemius were detected mitochondrial redox states respectively by using RRS. Sepsis was induced by cecal ligation and puncture (CLP). We applied RRS analysis at baseline and 30 min, 1 h, 2 h, 4 h, and 6 h after CLP, and

Peer review under responsibility of Cairo University.
* Corresponding author.
E-mail addresses: zhangzhanqin12@sina.com (Z. Zhang), dr.wangqiang@139.com (Q. Wang).

https://doi.org/10.1016/j.jare.2020.06.027

the mitochondrial redox states were identified. The levels of blood lactate as a predictor in sepsis were assessed. The predictive correlation of mitochondrial redox states on mortality, inflammation and organ dysfunction was further assessed.

Results: Mitochondrial redox states were clearly recognized in ex-vivo gastrocnemius muscles as well as purified mitochondria and primary skeletal muscle cells by using RRS. The peak area for the Raman reduced mitochondrial fraction, the indicator of mitochondrial redox states, fluctuated significantly at 2 h after CLP. This fluctuation occurred earlier than the change in lactate level. Moreover, this fluctuation had higher prognostic accuracy for mortality than the lactate level during sepsis and could be a novel diagnostic marker for predicting septic outcomes according to the cutoff value of 1.059, which had a sensitivity of 80% and a specificity of 90%.

Conclusions: This study demonstrated that monitoring mitochondrial redox states using RRS as early as 2 h could indicate outcomes in septic mice. These data may contribute to developing a non-invasive clinical device concerning mitochondrial redox states by using bedside-RRS.

Introduction

Sepsis is a life-threatening condition involving multiorgan dysfunction that has a rising mortality of approximately 6 million in critically ill patients [1,2]. Increased awareness and early detection of sepsis are important in reducing mortality with prompt use of evidence-based interventions [3]. The pathogenesis of mitochondrial damage as a result of sepsis probably involves a complex series of events [4–6]. Experimental evidence indicated that the emergence of mitochondrial dysfunction, including oxidative stress and energy metabolism, appeared early and was associated with the outcomes of sepsis [7,8]. However, most knowledge of mitochondrial function is hitherto derived from invasive laboratory examination by using isolated cells and mitochondria from biopsy specimens [6,8], which has restricted the clinical applications.

Resonance Raman spectroscopy (RRS) is a promising qualitative tool to analyze molecule vibrations and to identify molecular functions with structural fingerprints, even at negligibly low quantities [9–11]. Several studies have reported that RRS could be used to detect mitochondrial function in both isolated cells and tissues [11–13]. Takeshi *et al*. found that evaluation of mitochondrial function by using RRS displayed a similar sensitivity with noninvasive interference compared with other common mitochondrial function assays [12]. Recently, RRS has been used as a versatile diagnostic tool for detecting cancerous tissues in human patients [14]. Quantifying myocardial mitochondrial redox states on the epicardial surface *in vivo* by using RRS might permit the real-time identification of critical defects in organ-specific oxygen delivery and improve the accuracy of cardiac arrest prediction [11]. However, the application of RRS to detect mitochondrial dysfunction and its predictive value in sepsis are unclear.

Several researchers have noted that mitochondrial redox states may play a pivotal pathophysiological role in the development of sepsis-induced multiorgan dysfunction [6,15,16]. A recent clinical study showed that persistent low mitochondrial respiration was correlated with slower recovery from organ dysfunction in pediatric sepsis [15]. Mitochondrial function representing redox states in the skeletal muscle was severely impaired in septic patients and showed a good correlation with illness severity within 24 h after intensive care admission [16]. We hypothesized that visualizing mitochondrial redox status via RRS could identify the severity and prognosis of sepsis at an early stage. Therefore, we carried out an experimental study to determine whether this RRS tool could be a more effective indicator in monitoring mitochondrial redox states of gastrocnemius in sepsis and a more accurate predictor of septic outcomes than current methods.

Materials and methods

Animals

Adult male C57BL/6 mice (6–8 weeks old, weighing 22–25 g) were obtained from the Animal Center of Xi'an Jiaotong University (Xi'an, China) in this study. Mice were housed in pathogen-free cages under standardized conditions with a 12-hour light/dark cycle (lights on from 8:00 am to 8:00 pm) and free access to food and water. All animal experiments were approved by the Institutional Animal Care and Use Committee at Xi'an Jiaotong University (Xi'an, China).

Cecal ligation and puncture model

Cecal ligation and puncture (CLP) was performed as previously described [17]. Briefly, laparotomy was performed, and the cecum was gently exteriorized. Approximately 50% of the cecum was ligated using a 4-0 silk and double-punctured using a 21-gauge needle. A small amount (droplet) of feces was extruded from the surface of the cecum, and the peritoneum was closed. Then, the mice were resuscitated via subcutaneous injection of prewarmed 0.9% normal saline (5 ml/100g) and placed on a temperature-controlled pad until they regained independent mobility. Survival was continuously recorded for a total of 7 days. Blood pressure was measured by the tail cuff method using a BP-2000 blood pressure analysis system (Visitech Systems, Apex, NC, USA). Rectal temperature was recorded using a rectal probe thermometer.

Animal experimental protocol

This study included three experimental stages. In the first stage, mice (n = 7–29) were subjected to CLP to induce sepsis. Blood serum lactate was measured 1 h before CLP (baseline) and 2, 6, 12 and 24 h after CLP. RRS spectra were recorded 1 h before CLP (baseline) and 30 min and 1, 2, 4 and 6 h after CLP. Mitochondrial redox states, such as oxidized nicotinamide adenine dinucleotide (NAD^+), reduced nicotinamide adenine dinucleotide (NADH), and oxidized (GSSG) and reduced (GSH) glutathione, were detected. Blood serum lactate, high mobility group box 1 (HMGB1), procalcitonin (PCT), and C-reactive protein (CRP) were measured at 24 h post CLP. Correlations between RRS spectra and the parameters of sepsis were analyzed. In the second stage, a separate group of mice (n = 45) was subjected to CLP to induce sepsis. Raman spectra and blood serum lactate were recorded at 2 h after CLP. Survival was continuously recorded for a total of 7 days. The best cutoff value of the indicator extracted from RRS spectra to discriminate mortality was obtained using a receiver operating characteristic (ROC) curve. In the third stage, mice that underwent CLP were

divided into two groups (n = 5–8 per group) according to the cutoff value of 1.059: the less than 1.059 group (L group) and the more than or equal to 1.059 group (H group). The body weight, rectal temperature and blood systolic pressure were measured. The inflammatory response and multiorgan dysfunction were evaluated between the L group and the H group.

RRS study

RRS spectra in the spectral range of 600–1800 cm^{-1} were acquired using a Raman spectrometer (Horiba LabRAM HR Evolution, France) equipped with an Olympus BXFM open space optical microscope and a charge-coupled device detector. Resonance Raman spectra were recorded though an LWD50 × objective (NA = 0.5, WD = 10.6 mm) with a 532-nm Yd: NVO4 laser. The spot size of the analyzed area was approximately 1 μm in diameter. The calibration was performed using the silicon wafer Raman band at 520.7 cm^{-1}. The spectral resolution was 0.65 cm^{-1}. The accuracy of the wavenumber was ±0.03 cm^{-1}.

RRS spectra of mitochondria

Mitochondrial isolation was performed with a previously published method with slight modifications [18]. In brief, fresh mitochondria were obtained from the gastrocnemius of male C57BL/6 mice. The samples were washed with ice-cold relaxation buffer (100 mM KCl, 5 mM EGTA, 5 mM HEPES adjusted with KOH to pH 7.0) and then minced in the same buffer for 10 min. After resuspension with HES buffer (5 mM HEPES, 1 mM EDTA, 0.25 M sucrose, pH 7.4), the samples were homogenized using a glass dounce homogenizer and then centrifuged at 1000*g* for 10 min at 4 °C. The supernatant was collected and recentrifuged at 1000*g* for 10 min. The resulting supernatant was then centrifuged at 9000*g* for 15 min at 4 °C and resuspended in FFA-free HES buffer with 0.2% BSA. A small aliquot of purified mitochondria was reduced after the addition of a small amount of sodium dithionate (SDT, 10 mM, Sigma–Aldrich, MO, USA) to the mitochondrial solution. Raman spectra of the control (partially oxidized) and reduced mitochondria (n = 3–5 per group) were recorded at least 5 times with an acquisition time of 30 s and accumulation twice. The incident laser power on the samples was approximately 10 mW.

RRS spectra of skeletal muscle cells and tissues

Isolated primary skeletal muscle cells were prepared as previously described [19]. Mice were sacrificed by cervical dislocation. Then, the gastrocnemius of male C57BL/6 mice was harvested and minced in the culture medium. Primary skeletal muscle cells were prepared by enzymatic dissociation. The cells were cultured at 37 °C with a humidified atmosphere of 95% O_2 and 5% CO_2. For the Raman spectrum of cells, the culture medium was quickly removed and washed twice with HEPES-buffered Tyrode's solution (150 mM NaCl, 10 mM glucose, 10 mM HEPES, 4.0 mM KCl, 1.0 mM $MgCl_2$, 1.0 mM $CaCl_2$, and 4.0 mM NaOH). Then, the cells were fixed with 4 wt% paraformaldehyde in 0.1 M phosphate buffered saline for 10 min. After fixation, the Raman spectra of the cells were recorded. For the reduction-oxidation experiment, 10 mM SDT was added to the medium for 10 min, and the reduced form of the cell was observed with a Raman microscope. The Raman spectrum measurements were carried out on at least ten random points for each cell. For the control (partially oxidized) and reduced groups (n = 3 per group), more than three cells were recorded with an acquisition time of 20 s and accumulation once. The incident laser power on the sample was approximately 5 mW. The mentioned Raman spectra of each group are expressed as the average spectra.

For ex vivo measurement, the gastrocnemius muscle harvested from the right leg of male C57BL/6 mice was performed as previously described [20]. Then, the muscles were placed into a sterile dish with Krebs-Henseleit buffer (KHB) composed of 119 mM NaCl, 4.7 mM KCl, 2.5 mM $CaCl_2$, 1.2 mM $MgSO_4$, 1.2 mM KH_2PO_4 and 25 mM $NaHCO_3$ (pH 7.4). Raman spectra of the ex vivo gastrocnemius muscle were measured from at least five random spots using a laser power of approximately 25 mW. Signal collection was performed for 30 s, and accumulation was performed twice. To reduce ex vivo gastrocnemius muscle, we added a small amount of SDT (10 mM) to KHB for 10 min, and the Raman spectra were collected as described above.

RRS spectra in vivo

In the *in vivo* experiment, Raman spectra of the skeletal muscles of mice were recorded 1 h before CLP (baseline) and 30 min and 1, 2, 4 and 6 h after CLP. To prepare the "muscle" site, we shaved the right thigh and removed the hair, and the skin layer was cut and folded back with a fixed length away from the ankle to expose the gastrocnemius muscle, which was immediately detected by a Raman microscope in the measuring field of 9 mm^2. The laser power on the sample stage was 25 mW with an acquisition time of 15 s accumulating once. For each mouse, measurement was performed with at least 5 random points. Mice were anesthetized with inhalation of continuous low-dose isoflurane to allow a motionless and reliable Raman scan with comfortable care on a warmed pad (37℃) all the time. The "muscle" site was protected from injury and treated via a slight suture after measurement.

Raman spectra data processing

Raman spectra were processed using LabSpec6 software (Horiba JY) for each individual Raman spectrum. The mentioned Raman spectra of each sample are expressed as the average spectra. A linear baseline correction was applied to subtract the fluorescence background signal. The designed Raman peak from each spectrum was processed and fitted, and the peak areas were calculated using the LabSpec6 software suite.

Quantification of the bacterial burden of peritoneal lavage

The bacterial count was analyzed as previously described [21]. Twenty-four hours after CLP, 5 ml of sterile PBS was injected into the peritoneal cavities of the mice. After gentle mixing, 4 ml of this peritoneal lavage fluid was collected. Then, after serial dilutions, bacterial counts were determined by incubating 100 μl of the samples with these dilutions on tryptic soy agar plates followed by incubation at 37 °C for 24 h. Colony forming units were counted and are expressed as log10 of units per milliliter.

Hematoxylin-eosin staining and analysis

The lung, kidney, liver, and heart were collected at 24 h post-CLP. Then, the tissues were immediately fixed in 4 wt% paraformaldehyde and dehydrated in a gradient ethanol series. These tissues were sliced into sections at a thickness of 5 μm with paraffin embedding and stained with hematoxylin-eosin (Boster Bioengineering, Inc., Wuhan, Hubei, China). Histological examination was performed via an Olympus CX23 microscope (Olympus, Shinjuku, Tokyo, Japan). Evaluation of the tissue pathological severity was performed blindly and scored using a semiquantitative scoring system as previously described [22,23]. The histology injury scores are expressed as the sum of the individual scores. In detail, the lung was scored on parameters including alveolar congestion, hemorrhage, neutrophil or leukocyte infiltration, and

cellular hyperplasia. The parameters of kidney injury were tissue necrosis, tubular atrophy, leukocyte infiltration in the glomeruli and tubular cast formation. Liver injury was scored on the presence of hepatocyte vacuolization, cell necrosis and nuclear fragmentation. Heart injury was scored based on the presence of myocardial fibers, obscure nucleus/karyopyknosis, interstitial lymphocyte infiltration and lytic necrosis.

Lung wet-to-dry weight ratio

For quantification of the magnitude of pulmonary edema, lung tissues were harvested, and the wet weight was immediately recorded. The lung was placed in an oven at 60 °C for 48 h until the weight was constant, and then, it was reweighed to determine the dry weight. The lung water content was calculated as the ratio of wet weight to dry weight as follows: W/D ratio = wet weight − dry weight/dry weight.

Organ function analysis and cytokines/chemokines

Approximately 0.1 ml of blood was collected from the tail vein at a defined time after CLP for every biochemical assay in this study. After centrifugation (3000 rpm, 15 min, 4 °C), the serum was removed and stored at −80 °C for analysis. Serum PCT, CRP, cardiac troponin I (cTnI) (USCN Life Science, Inc., Wuhan, China) and HMGB1 (Cusabio Biotech Co., Ltd., Wuhan, China) levels were determined using specific enzyme-linked immunoassay (ELISA) kits following the manufacturer's instructions. The concentrations of interleukin-6 (IL-6), interleukin-10 (IL-10) and tumor necrosis factor-α (TNF-α) were quantified using ELISA kits (Arigo Biolaboratories, Hsinchu City, Taiwan, China). The serum levels of alanine transaminase (ALT), aspartate transaminase (AST), blood urea nitrogen (BUN) and creatinine (Cre) were used as indicators for liver and kidney function and were measured with a biochemistry automatic analyzer (Chemray 240, Rayto Life and Analytical Sciences Co., Ltd., China). Serum lactate was detected using the Lactate Assay Kit (Arigo Biolaboratories, Hsinchu City, Taiwan, China).

NAD^+/NADH and GSH/GSSG analysis

After Raman detection, the control and reduced forms of mitochondria (processed with SDT) were rapidly stored in liquid nitrogen for further experiments (n = 3–5 per group). For skeletal muscle analysis, the gastrocnemius detected by Raman spectroscopy was quickly harvested and stored in liquid nitrogen (n = 16 mice). The NAD^+ and NADH contents were measured by an NAD/NADH assay (BioAssay Systems, Hayward, CA) according to the manufacturer's instructions. GSSG and GSH were measured in the mitochondria and homogenate of skeletal muscles using a GSH/GSSG Ratio Detection Assay Kit (Abcam, Cambridge, MA, USA).

Statistical analysis

All data analysis was performed using SPSS Statistics version 22.0 for Windows (IBM Co., Armonk, NY, USA) and GraphPad Prism version 8.00 for Windows (GraphPad Software, Inc., La Jolla, CA, USA). Unpaired two-tailed Student's *t* test was performed to compare mean values between two groups at a single time point. In repeated measurements, one-way ANOVA tests were performed followed by Dunnett's multiple comparison post-test. Two-way ANOVA with Sidak's multiple-comparison test was used to compare the parameters based on timing and groups after sepsis. Pearson's or Spearman correlation analysis was used as appropriate to detect correlation coefficients. ROC analysis was performed to assess the diagnostic performance. Values are expressed as the mean ± SEM. Statistical significance was set as $p < 0.05$.

Results

Visualizing mitochondrial redox states by resonance-enhanced Raman bands

To determine whether RRS could identify mitochondrial redox states, we used 532 nm laser excitation to obtain the RRS spectrum of major mitochondrial components within the fingerprint region at the subcellular, cellular and tissue levels. We observed significantly increased intensity near the characteristic redox peak at 750 cm^{-1} in the RRS spectrum of the mitochondrial reduced form (SDT group) compared with the partially oxidized form (control group) (Fig. 1A, B; (1)). Increased Raman peak intensity at 750 cm^{-1} was associated with reduced NAD^+ and GSSG concentrations (Fig. 1C). In addition, our analysis of RRS spectra in ex vivo gastrocnemius as well as primary skeletal muscle cells produced consistent results (Fig. 1A, B; (2), (3)). There were also intensive peaks at 1128 and 1585 cm^{-1} showing similar fluctuations compared to that at 750 cm^{-1} (Fig. 1A, B). Original RRS spectra are shown in Suppl. Fig. 1A. Overall, we could identify the changed mitochondrial redox states in muscle tissues directly by RRS.

Changes in the mitochondrial redox states were detected early using RRS in vivo

A moderate CLP model with an accumulated mortality rate of 58.9% within 7 days was used (Fig. 2A). As shown in Fig. 2B, the blood lactate level had a slight trend of increase at 6 h and was significantly elevated at 12 h ($p < 0.05$) post-CLP. Accordingly, we attained RRS spectra at a series of intervals for early detection of septic outcomes (Fig. 2D). The original RRS spectra are shown in Suppl. Fig. 1B. Mitochondrial redox states were quantified by normalizing the spectral peak area under 750 cm^{-1} to that under the 1004 cm^{-1} peak, and this metric was summarized as the peak area for the Raman reduced mitochondrial fraction (PA-2RMF). Specifically, PA-2RMF showed a change as early as 2 h ($p < 0.05$) and maintained this level after 4 h and 6 h in septic mice (Fig. 2C). These results indicated that PA-2RMF yielded an earlier change following CLP surgery than the blood lactate level (Suppl. Fig. 1).

Because PA-2RMF changed 2 h after CLP, the ratio of PA-2RMF from 2 h to baseline was chosen to evaluate the change in mitochondrial redox states during sepsis, defined as RPA-$2RMF_{2h}$. As shown in Fig. 2E–G, RPA-$2RMF_{2h}$ had a positive correlation with NAD^+ content and the ratios of NAD^+/NADH and GSH/GSSG ($r = 0.6275$, $p = 0.0093$; $r = 0.5294$, $p = 0.0349$; $r = 0.5084$, $p = 0.0443$). Overall, RPA-$2RMF_{2h}$ could be a highly potent indicator of mitochondrial redox states as early as 2 h after CLP.

Analysis of mitochondrial redox state to discriminate mortality in murine sepsis

To determine the association between RPA-$2RMF_{2h}$ and parameters of infection or organ dysfunction, we assessed the statistical correlations. RPA-$2RMF_{2h}$ showed a negative correlation with blood lactate, HMGB1, PCT and CRP levels at 24 h after CLP ($r = -0.4298$, $p = 0.0406$; $r = -0.4792$, $p = 0.0114$; $r = -0.4006$, $p = 0.0313$; $r = -0.4083$, $p = 0.0279$; Fig. 3A–D). However, these parameters were not correlated with the blood lactate level at 2 h post CLP (Suppl. Fig. 2A–D).

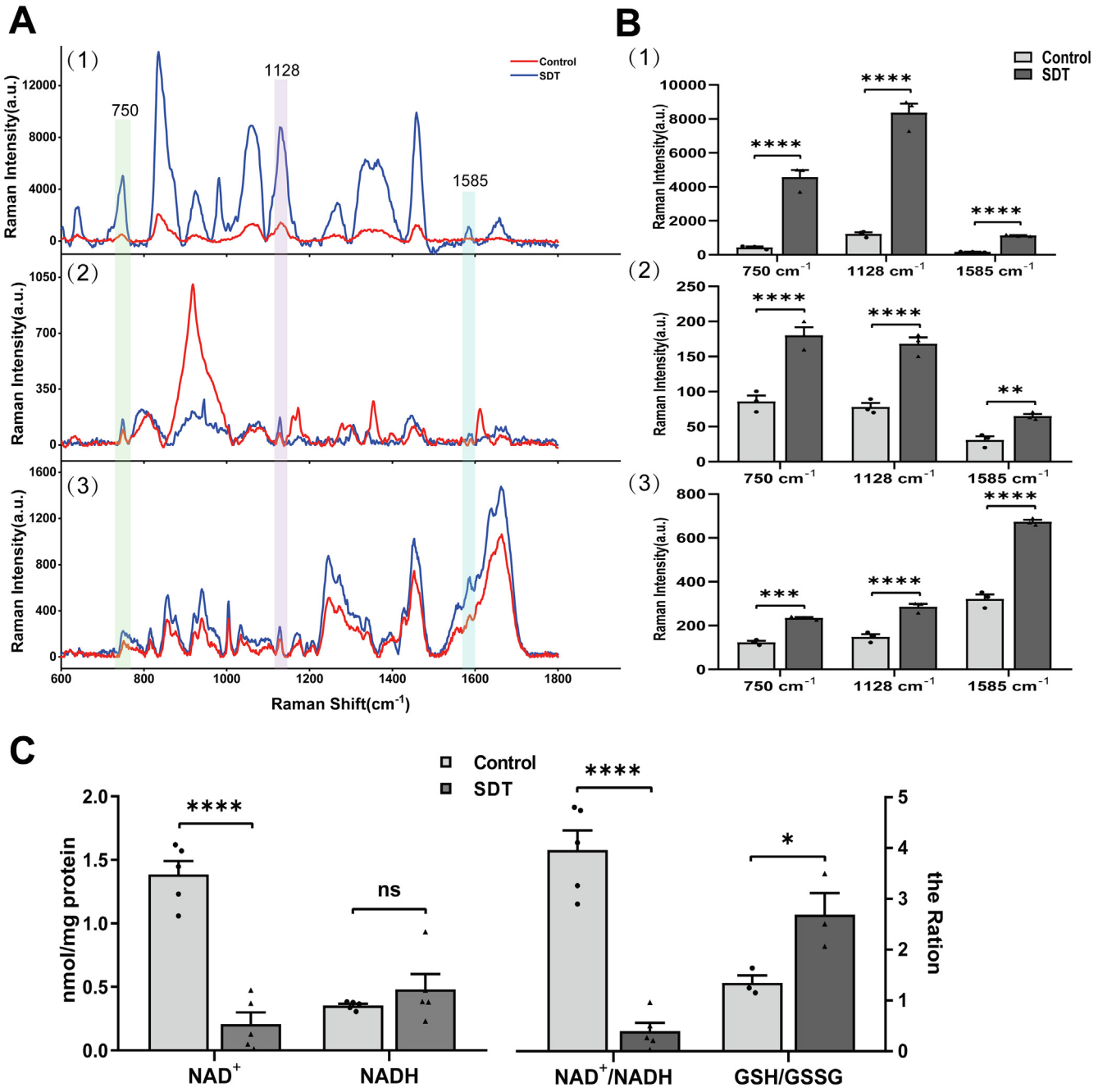

Fig. 1. Resonance Raman spectra during manipulation of the mitochondrial redox state, (A) Raman spectrum of (1) mitochondria, (2) primary skeletal muscle cells and (3) ex vivo gastrocnemius muscles before and after adding the strong reductant sodium dithionate (SDT). Blue lines represent reduced species (SDT group), and red lines represent normal species (control group). (B) Effect of redox reaction on the intensity of the mitochondrial peaks at 750, 1128 and 1585 cm^{-1} in (1) mitochondria, (2) primary skeletal muscle cells and (3) ex vivo gastrocnemius muscles. n = 3 per group. (C) Comparisons of the NAD^+ and NADH levels and the NAD^+/NADH (n = 5 per group) and GSH to GSSG ratios (n = 3 per group) in mitochondria between the control and SDT groups. Data are expressed as the mean ± SEM and analyzed by Student's *t* test. $^*p < 0.05$, $^{**}p < 0.01$, $^{***}p < 0.001$, $^{****}p < 0.0001$ compared with the control group. NAD^+ = oxidized nicotinamide adenine dinucleotide, NADH = reduced nicotinamide adenine dinucleotide, GSSG = oxidized glutathione, GSH = reduced glutathione, ns = no significance.

Then, a ROC curve was applied to determine the accuracy of RPA-$2RMF_{2h}$ for predicting mortality. As illustrated in Fig. 3E, the area under the curve of RPA-$2RMF_{2h}$ was 0.880 (95% CI: 0.736–1.000, p = 0003). However, the AUC for the blood lactate level 2 h after CLP was 0.621 (95% CI: 0.374–0.869, p = 0.246, Suppl. Fig. 2E). RPA-$2RMF_{2h}$ had higher prognostic accuracy of mortality than lactate level during sepsis (p = 0.037). As noted, the optimal cutoff of RPA-$2RMF_{2h}$ levels for predicting mortality was 1.059 with a sensitivity of 80% and a specificity of 90% (Fig. 3F).

Mitochondrial redox states associated with cytokine production and bacterial loading in sepsis

Mice that underwent CLP were divided into two groups according to the RPA-$2RMF_{2h}$ cutoff value of 1.059: the RPA-$2RMF_{2h}$ < 1.059 group (L group) and the RPA-$2RMF_{2h}$ ≥ 1.059 group (H group). The changes in body weight, rectal temperature and blood systolic pressure were compared (Fig. 4A–C). Importantly, Fig. 4D shows that mice exhibited a higher peritoneal lavage bacterial loading in the L group than in the H group at

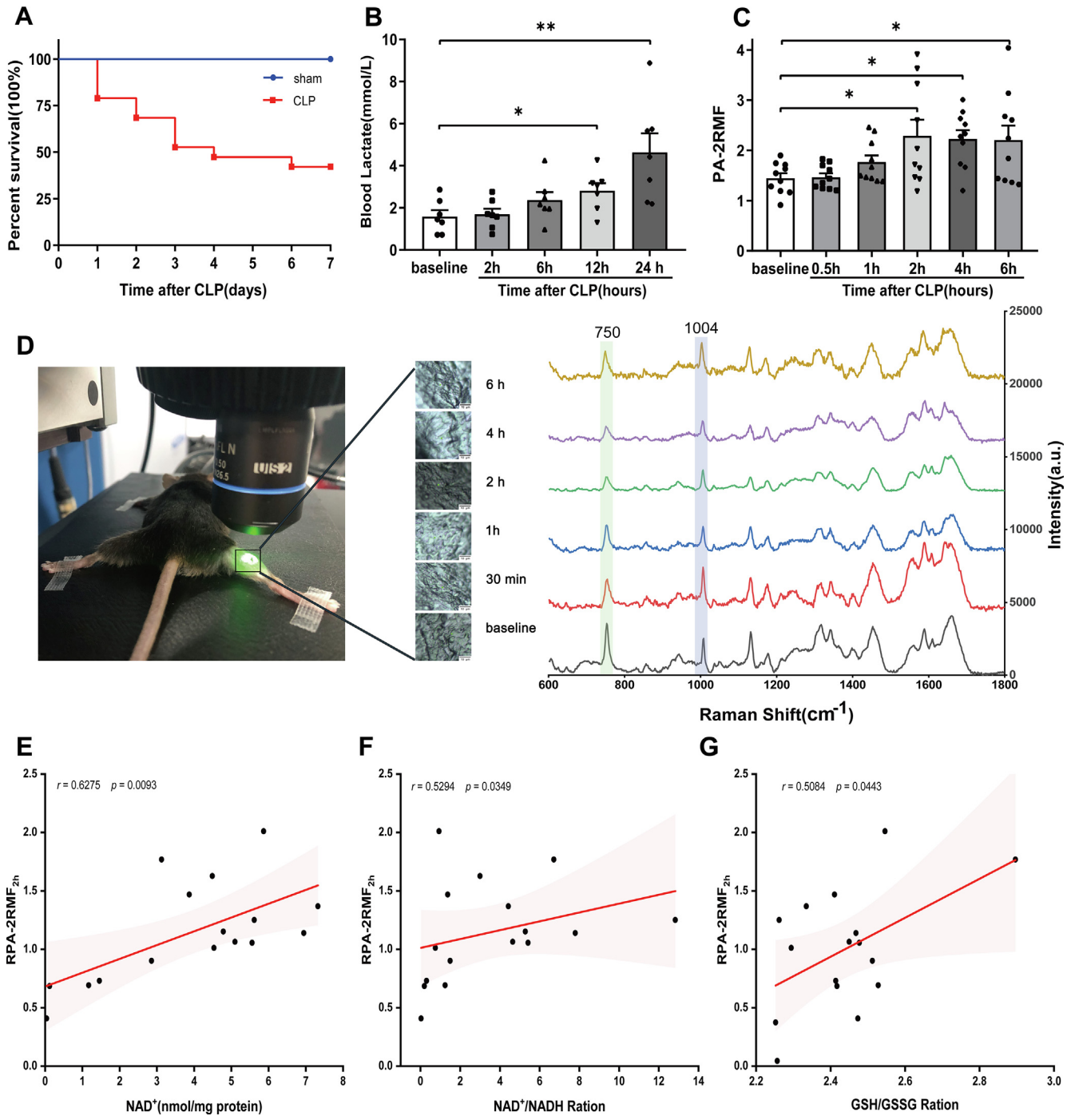

Fig. 2. Changes in mitochondrial redox states were detected early using resonance Raman spectroscopy *in vivo*, (A) The survival rate was monitored between the CLP group and the sham group. n = 16–19 mice per group. (B) Levels of serum lactate at baseline (1 h before CLP) and 2 h, 6 h, 12 h and 24 h after CLP. n = 7 mice per group. (C) Peak area for the Raman reduced mitochondrial fraction (PA-2RMF) at the different time points (baseline, 30 min, 1 h, 2 h, 4 h, 6 h after CLP). n = 10 mice per group, 0.5 h = 30 min. (D) Skeletal muscle position with respect to the objective and laser light for Raman spectrum measurement in CLP-induced sepsis *in vivo*. The mouse was fixed in a warmed black pad (37 °C). The Raman spectra were collected at baseline (1 h before CLP) and 30 min, 1 h, 2 h, 4 h and 6 h after CLP. Light field (scale bars, 10 μm). (E)-(G) Correlation between the ratio of PA-2RMF from 2 h after CLP to baseline ($RPA\text{-}2RMF_{2h}$) and the NAD^+, NAD^+/NADH or GSH/GSSG levels in the gastrocnemius muscle of septic mice. n = 16 mice per group. Data are expressed as the mean ± SEM. Comparisons between groups were analyzed by one-way ANOVA with Dunnett's multiple comparison post-test. The Pearson correlation coefficient was used to assess the correlation between $PA\text{-}2RMG_{2h}$ and mitochondrial redox status parameters. $^*p < 0.05$, $^{**}p < 0.01$ compared with the baseline group. CLP = cecal ligation and puncture, NAD^+ = oxidized nicotinamide adenine dinucleotide, NADH = reduced nicotinamide adenine dinucleotide, GSSG = oxidized glutathione, GSH = reduced glutathione.

24 h post CLP ($p < 0.001$). Compared with those at baseline, the levels of IL-6 and TNF-α showed a substantial increase in the L group ($p < 0.05$ or $p < 0.001$, Fig. 4E). In addition, significant differences in the IL-6, IL-10 and TNF-α levels between the L group and H group were observed at 24 h after CLP ($p < 0.05$ or $p < 0.01$, Fig. 4E).

Mitochondrial redox states related to multiorgan dysfunction of sepsis

We further found that the HMGB1, CRP and PCT levels were significantly higher in the L group than in the H group at 24 h after CLP ($p < 0.01$, Fig. 5). In addition, histologic examination was performed. As illustrated in Fig. 6A, the lung tissues showed alveolar

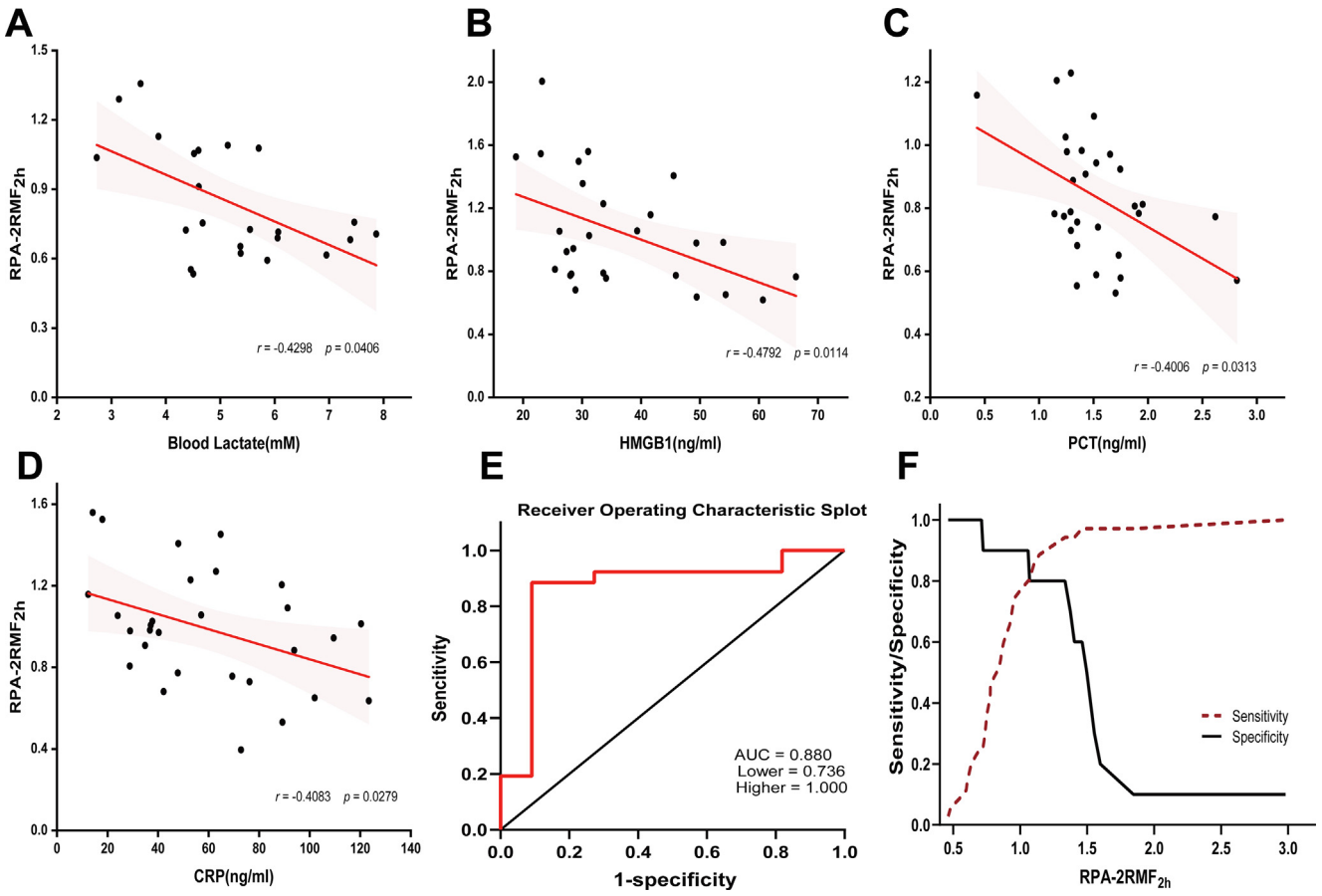

Fig. 3. Performance of mitochondrial redox states using resonance Raman spectroscopy for septic mortality, (A)-(D) Correlation between the ratio of PA-2RMF from 2 h after CLP to baseline (RPA-2RMF$_{2h}$) and the parameters of sepsis including blood serum lactate, high mobility group box 1 (HMGB1), procalcitonin (PCT), and C-reactive protein (CRP) at 24 h post CLP. n = 23–29 mice per group. Pearson or Spearman correlation coefficients were used to assess the correlation between PA-2RMF$_{2h}$ and these parameters of sepsis. (E) Receiver operating characteristic curve of RPA-2RMF$_{2h}$ (solid red, AUC = 0.88, n = 45) as a diagnostic test for predicting mortality in sepsis. (F) Sensitivity (dotted red) and specificity (solid black) of the RPA-2RMF$_{2h}$ values for predicting mortality in sepsis within 7 days after CLP. CLP = cecal ligation and puncture, AUC = area under the curve.

congestion and inflammatory cell accumulation, as well as impaired alveoli; interstitial lymphocyte infiltration, coagulative necrosis and lytic necrosis were observed in the heart; the renal sections revealed glomerular destruction, leukocyte infiltration in the glomeruli and tubular cast formation; and liver histopathology showed disappearance of sinus hepaticus, increased hepatocyte vacuolization and cell necrosis in the L group. However, there were mild histological changes in the H group. The histologic organ injury scores were compared between the H group and the L group (Fig. 6B). There was no significant difference in the serum concentrations of AST (Fig. 6E). However, sepsis-induced multiorgan injury was indicated by the increased lung wet-to-dry weight ratio and the cTnI, BUN, Cre and ALT levels in the L group versus the H group at 24 h post CLP (Fig. 6C–E).

Discussion

In CLP-induced sepsis, our method provides a novel and potential indicator for early identification of the outcomes of sepsis via the quantification of mitochondrial redox states by using RRS. The redox state indicator of mitochondria extracted from RRS spectra (RPA-2RMF$_{2h}$) as early as 2 h after CLP injury could predict mortality with high prognostic accuracy and identify the disturbed inflammatory response and multiorgan dysfunction in septic mice.

Previous studies have shown that septic patients with disturbed mitochondrial redox states had poor outcomes with high mortality [15,16]. Similar results were observed in this study, in which the mitochondrial redox state based on RRS indicated the outcomes of sepsis, including inflammation, multiorgan dysfunction and mortality of sepsis. As hypothesized, RRS allowed early detection of mitochondrial redox states during sepsis in accordance with common assays of mitochondrial redox state activity, such as NAD^+/NADH and GSH measurements, representing cellular redox homeostasis.

Mitochondrial cytochromes can represent mitochondrial redox states carrying out electron transport in the electron transport chain [24,25]. RRS accurately identified the characteristic peaks at 750 cm^{-1}, 1128 cm^{-1} and 1585 cm^{-1}, which are assigned to symmetric vibrations of porphyrin, vibrations of C_b-CH3 side radicals and vibrations of methine bridges (C_aC_m, C_aC_mH bonds), as previously described [26,27]. All of them are sensitive to the redox state of cytochromes and mainly contribute to cytochrome (cyt) c and cyt b [26]. In addition, the resonance-enhanced Raman band at 750 cm^{-1} has already been used in the detection of mitochondrial redox states [12]. Moreover, the band 1585 cm^{-1} may overlap the band of other proteins [13]. Therefore, the 750 cm^{-1} general cytochrome band was chosen to visualize mitochondrial redox states in this study. The Raman band located at 1004 cm^{-1} corresponds to the breathing mode of phenylalanine [28]. Here, the area under the 1004 cm^{-1} peak was set as a reference to quantify mitochondrial redox states, as it shows the stable conformational changes of proteins to normalize spectra.

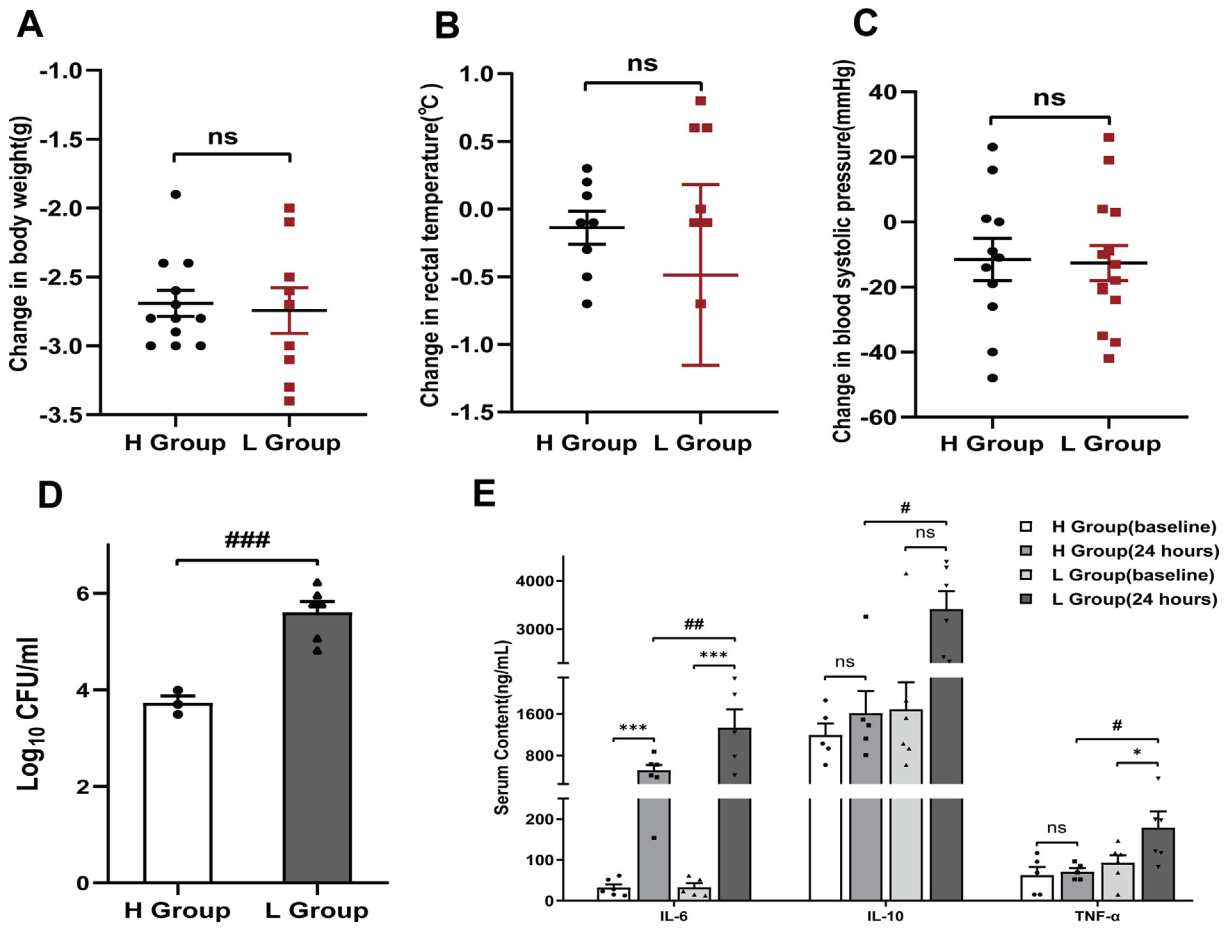

Fig. 4. Measurement of inflammatory cytokines and bacterial loading associated with mitochondrial redox states in septic mice, (A)-(C) Changes in the body weight, rectal temperature and blood systolic pressure in the H group and the L group. (D) Colony-forming units (CFUs) in the peritoneal lavage were counted 24 h post CLP in mice from the H group and the L group. n = 3 or 5 per group. (E) Concentrations of the inflammatory cytokines interleukin (IL)-6, IL-10 and tumor necrosis factor (TNF)-α in the serum samples at baseline (1 h before CLP) and 24 h post CLP in the H group and the L group. n = 5–6 per group. Data are expressed as the mean ± SEM and were analyzed by Student's *t* test or two-way ANOVA with multiple-comparison testing. $^{*}p < 0.05$, $^{**}p < 0.01$, $^{***}p < 0.001$, $^{****}p < 0.0001$ compared with the baseline group, $^{\#}p < 0.05$, $^{\#\#}p < 0.01$, $^{\#\#\#}p < 0.001$ compared with the H group at 24 h post CLP. H group = the ratio of PA-2RMF from 2 h after CLP to baseline ($RPA\text{-}2RMF_{2h}$) was at or exceeded 1.0059, L group = $RPA\text{-}2RMF_{2h}$ was below 1. 0059, ns = no significance, CLP = cecal ligation and puncture.

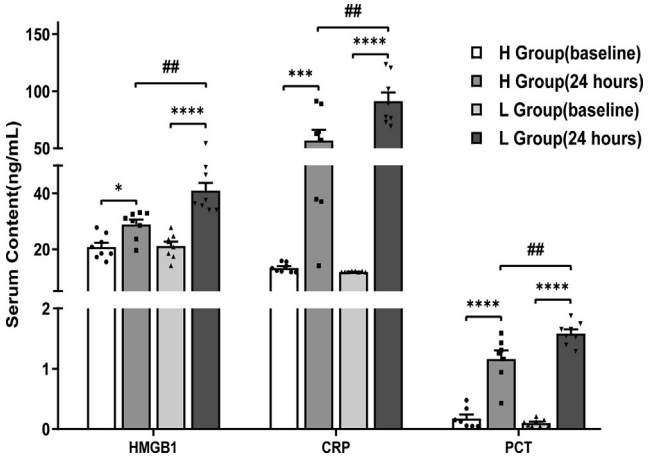

Fig. 5. Levels of high mobility group box 1 (HMGB1), C-reactive protein (CRP) and procalcitonin (PCT) at baseline and 24 h post CLP in the H group and the L group. n = 7 or 8 per group. Data are expressed as the mean ± SEM and were analyzed by Student's *t* test or two-way ANOVA with multiple-comparison testing. $^{*}p < 0.05$, $^{**}p < 0.01$, $^{***}p < 0.001$, $^{****}p < 0.0001$ compared with the baseline group, $^{\#}p < 0.05$, $^{\#\#}p < 0.01$, $^{\#\#\#}p < 0.001$ compared with the H group at 24 h post CLP. H group = the ratio of PA-2RMF from 2 h after CLP to baseline ($RPA\text{-}2RMF_{2h}$) was at or exceeded 1.0059, L group = $RPA\text{-}2RMF_{2h}$ was below 1. 0059, ns = no significance, CLP = cecal ligation and puncture.

To date, measurement of mitochondrial dysfunction in sepsis relies on tissue biopsies using common biochemical tools, which may damage the mitochondria *in vivo* [6,29]. However, noninvasive monitoring of the redox states of intact mitochondria could be achievable *in vivo* by RRS without any damage. In contrast, blood lactate level has a confirmed relationship with mortality as a bundle element for risk assessment and guides therapy according to the Surviving Sepsis Campaign guidelines [30]. However, blood lactate is a delayed surrogate index of hypoperfusion [31]. Septic patients with normal lactate concentrations still suffer from poor prognosis, and lactate clearance-guided therapy is not always successful in the clinic [32]. Surprisingly, our results indicated that the PA-2RMF value changed 2 h earlier than the blood lactate level in septic mice and was a superior indicator of septic outcomes.

Conservatively, the mortality of CLP-induced sepsis in this study was set to approximately 50% (actually 58.9%) within 7 days after CLP. There were several reasons for this decision. First, it was reported that the incidence of septic patient deaths in the intensive care unit fluctuated from 20% to 60% [33]. To closely reproduce clinical data and improve clinical translation, we chose CLP-induced moderate sepsis to yield high-quality experimental data. Second, mortality was a vital index of sepsis in our study. This selection guaranteed an adequate number of both dead and alive mice to avoid the bias caused by models and followed the goals

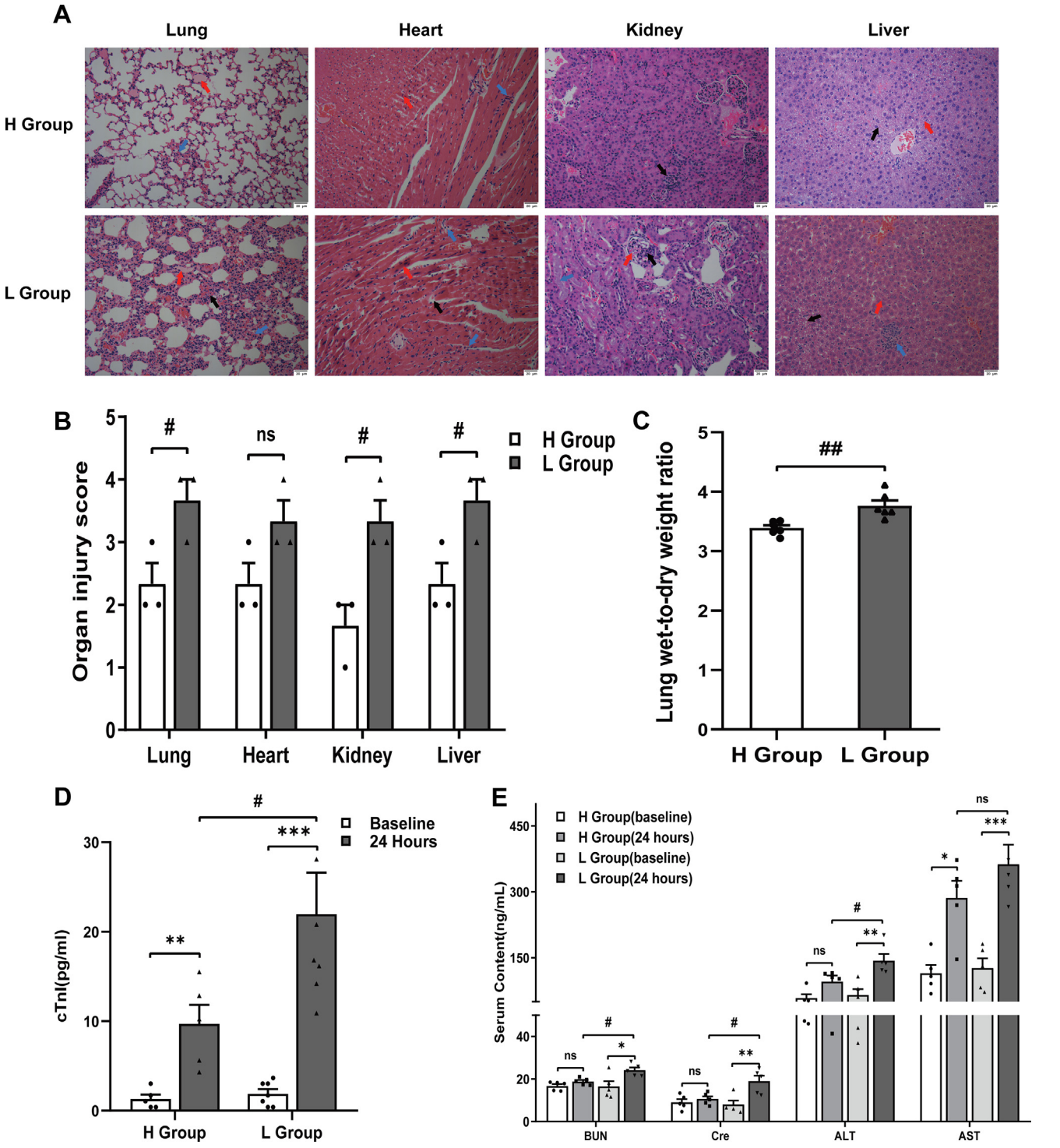

Fig. 6. Organ function assessment associated with mitochondrial redox states in septic mice, (A) Representative hematoxylin-eosin sections of the lung, heart, kidney and liver in the H group and L group are shown at ×200 original magnification, and the scale bars are 20 μm. In lung histology, the red arrow indicates alveolar congestion and infiltrated inflammatory cells in the alveoli, the blue arrow indicates alveolar wall thickening, and the black arrow indicates enlarged interstitial space. In heart sections, the red arrow indicates coagulative necrosis, the blue arrow indicates interstitial lymphocyte infiltration, and the black arrow indicates lytic necrosis. The kidney tissues demonstrated leukocyte infiltration in glomeruli (black arrow), glomerular destruction (red arrow) and tubular proteinaceous casts (blue arrow). Histologic analysis of the liver showed disappearance of the sinus hepaticus (red arrow), hepatocyte vacuolization (black arrow) and cell necrosis (blue arrow). (B) Quantification of the lung, heart, kidney and hepatic injury scores are presented. n = 3 per group. (C) Lung wet-to-dry weight ratio analysis. (D), (E) Serum marker levels of organ injury at baseline and 24 h post CLP in the H group and the L group were analyzed with the following: (D) cardiac troponin I (cTnI); (E) blood urea nitrogen (BUN), creatinine (Cre), alanine aminotransferase (ALT) and aspartate aminotransferase (AST). n = 5–7 per group. Data are expressed as the mean ± SEM and were analyzed by Student's *t* test or two-way ANOVA with multiple-comparison testing. $^{*}p < 0.05$, $^{**}p < 0.01$, $^{***}p < 0.001$ compared with the baseline group, $^{\#}p < 0.05$, $^{\#\#}p < 0.01$ compared with the H group at 24 h post CLP. H group = the ratio of PA-2RMF from 2 h after CLP to baseline ($RPA\text{-}2RMF_{2h}$) was at or exceeded 1.0059, L group = $RPA\text{-}2RMF_{2h}$ was below 1. 0059, ns = no significance, CLP = cecal ligation and puncture. (For interpretation of the references to colour in this figure legend, the reader is referred to the web version of this article.)

of the "Three Rs" to improve animal welfare by maximizing the utility of mice. Finally, the predictive value of biomarkers might be artificially enhanced in highly lethal CLP models [34].

Given that impulses arising from blood vessels could affect the RRS measurement, a relatively small measuring field of 9 mm^2 away from blood vessels in the muscle was chosen for screening, and the RRS spectrum was collected at a minimum of 5 random points with each operation focused on obtaining a rigorously high-quality spectrum. The mice were in an unconstrained prone position to allow extension of the right hind limb. The muscles were directly exposed to conduct RRS measurement to completely avoid the interference of skin and subcutaneous tissue in this study. With the development of tissue transparency [35], visualizing the mitochondrial redox state of skeletal muscles at the surface of skin using RRS is possible.

Further progress is still needed. First, RRS is currently used to detect the reduced cytochromes, as the Raman scatter of the oxidized cytochromes is negligible under 532 nm excitation [36]. However, constant extraction of oxidized cytochrome Raman bands to further assess mitochondrial redox states is an important issue. Furthermore, cyt c and cyt b are the major cytochrome components in mitochondria by resonance-enhancement effects using 532 nm excitation [26,37]. However, it is difficult to distinguish which one is reduced during sepsis because both are essential components of the respiratory electron transport chain. In addition, the 532 nm laser used here allowed tissue penetration of no more than 2 mm, which made it difficult to acquire further information *in vivo* and revealed only partial mitochondrial function in the area of penetration [38]. Finally, the *in vivo* evaluation in this study required operative exposure of the muscle evaluated, an intervention with obvious limitations in clinical practice. However, RRS for noninvasive and label-free measurement, which may reflect the *in vivo* mitochondrial redox status for the evaluation of mitochondrial function in sepsis, might be valuable for predicting septic outcomes in the clinic and provide a biomarker that can be a specific target of an adjunctive treatment.

Conclusions

In conclusion, this study demonstrated that monitoring mitochondrial redox states using RRS as early as 2 h could indicate outcomes in septic mice. This indicator was observed earlier than the blood lactate level and had a good correlation with the inflammatory response, multiorgan dysfunction and mortality of sepsis. In addition, our study showed that RRS could detect mitochondrial dysfunction in sepsis and provide a biomarker that can be a specific target of adjunctive treatment. These data suggested that developing mitochondrial redox state monitoring systems using RRS may potentially lead to a novel risk stratification and therapy management of sepsis at the bedside.

Compliance with Ethics Requirements

All animal experiments received the approval of the Institutional Animal Care and Use Committee at Xi'an Jiaotong University (approval no. 2018106).

Declaration of Competing Interest

The authors declare that they have no known competing financial interests or personal relationships that could have appeared to influence the work reported in this paper.

Acknowledgments

The authors gratefully acknowledge the Instrumental Analysis Center of Xi'an Jiaotong University for strong support for our usage of Raman spectroscopy and senior engineer Yu Wang from the Instrumental Analysis Center of Xi'an Jiaotong University for assistance with the Raman spectra data acquisition and analysis. This study was supported by programs from the National Natural Science Foundation of China (Nos. 81774113, 81974540, and 81801958), Beijing, China, and the Natural Science Basic Research Plan in Shaanxi Province of China (No. 2019JQ-352), Xi'an, Shaanxi, China.

Appendix A. Supplementary material

Supplementary data to this article can be found online at https://doi.org/10.1016/j.jare.2020.06.027.

References

[1] Rhodes A, Evans LE, Alhazzani W, Levy MM, Antonelli M, Ferrer R, et al. Surviving sepsis campaign: international guidelines for management of sepsis and septic shock: 2016. Crit Care Med 2017;45:486–552.
[2] Fleischmann C, Scherag A, Adhikari NK, Hartog CS, Tsaganos T, Schlattmann P, et al. Assessment of global incidence and mortality of hospital-treated sepsis. Current estimates and limitations. Am J Respir Crit Care Med 2016;193:259–72.
[3] Liu VX, Fielding-Singh V, Greene JD, Baker JM, Iwashyna TJ, Bhattacharya J, et al. The timing of early antibiotics and hospital mortality in sepsis. Am J Respir Crit Care Med 2017;196:856–63.
[4] Singer M. The role of mitochondrial dysfunction in sepsis-induced multi-organ failure. Virulence 2014;5:66–72.
[5] Fink MP. Cytopathic hypoxia. Is oxygen use impaired in sepsis as a result of an acquired intrinsic derangement in cellular respiration?. Crit Care Clin 2002;18:165–75.
[6] Galley HF. Oxidative stress and mitochondrial dysfunction in sepsis. Br J Anaesth 2011;107:57–64.
[7] Crouser ED, Julian MW, Huff JE, Struck J, Cook CH. Carbamoyl phosphate synthase-1: a marker of mitochondrial damage and depletion in the liver during sepsis. Crit Care Med 2006;34:2439–46.
[8] Carre JE, Orban JC, Re L, Felsmann K, Iffert W, Bauer M, et al. Survival in critical illness is associated with early activation of mitochondrial biogenesis. Am J Respir Crit Care Med 2010;182:745–51.
[9] Spiro TG. Resonance Raman spectroscopy. New structure probe for biological chromophores. Acc Chem Res 1974; 7: 339–344.
[10] Spiro TG, Strekas TC. Resonance Raman spectra of hemoglobin and cytochrome c: inverse polarization and vibronic scattering. Proc Natl Acad Sci USA 1972;69:2622–6.
[11] Perry DA, Salvin JW, Romfh P, Chen P, Krishnamurthy K, Thomson LM, et al. Responsive monitoring of mitochondrial redox states in heart muscle predicts impending cardiac arrest. Sci Transl Med 2017;9:eaan0117.
[12] Morimoto T, Chiu LD, Kanda H, Kawagoe H, Ozawa T, Nakamura M, et al. Using redox-sensitive mitochondrial cytochrome Raman bands for label-free detection of mitochondrial dysfunction. Analyst 2019;144:2531–40.
[13] Brazhe NA, Treiman M, Faricelli B, Vestergaard JH, Sosnovtseva O. In situ Raman study of redox state changes of mitochondrial cytochromes in a perfused rat heart. PLoS ONE 2013;8:e70488.
[14] Zhou Y, Liu C-h, Sun Y, Pu Y, Boydston-White S, Liu Y, et al. Human brain cancer studied by resonance Raman spectroscopy. J Biomed Opt 2012;17:116021.
[15] Weiss SL, Zhang D, Bush J, Graham K, Starr J, Tuluc F, et al. Persistent mitochondrial dysfunction linked to prolonged organ dysfunction in pediatric sepsis. Crit Care Med 2019;47:1433–41.
[16] Brealey D, Brand M, Hargreaves I, Heales S, Land J, Smolenski R, et al. Association between mitochondrial dysfunction and severity and outcome of septic shock. Lancet 2002;360:219–23.
[17] Rittirsch D, Huber-Lang MS, Flierl MA, Ward PA. Immunodesign of experimental sepsis by cecal ligation and puncture. Nat Protoc 2009;4:31–6.
[18] Preble JM, Pacak CA, Kondo H, MacKay AA, Cowan DB, McCully JD. Rapid isolation and purification of mitochondria for transplantation by tissue dissociation and differential filtration. J Vis Exp 2014:e51682.
[19] Hindi L, McMillan JD, Afroze D, Hindi SM, Kumar A. Isolation, culturing, and differentiation of primary myoblasts from skeletal muscle of adult mice. Biol Protoc 2017;7:e2248.
[20] Nagy JA, DiDonato CJ, Rutkove SB, Sanchez B. Permittivity of ex vivo healthy and diseased murine skeletal muscle from 10 kHz to 1 MHz. Sci Data 2019;6:37.
[21] Chen Q, Zhang K, Jin Y, Zhu T, Cheng B, Shu Q, et al. Triggering receptor expressed on myeloid cells-2 protects against polymicrobial sepsis by enhancing bacterial clearance. Am J Respir Crit Care Med 2013;188:201–12.

[22] Yang W-L, Ma G, Zhou M, Aziz M, Yen H-T, Marvropoulos SA, et al. Combined administration of human ghrelin and human growth hormone attenuates organ injury and improves survival in aged septic rats. Mol Med 2016;22:124–35.
[23] Li H, Wang S, Zhan B, He W, Chu L, Qiu D, et al. Therapeutic effect of Schistosoma japonicum cystatin on bacterial sepsis in mice. Parasites Vectors 2017;10. 222-222.
[24] Mitchell P. Coupling of phosphorylation to electron and hydrogen transfer by a chemi-osmotic type of mechanism. Nature 1961;191:144–8.
[25] Fernie AR, Carrari F, Sweetlove LJ. Respiratory metabolism: glycolysis, the TCA cycle and mitochondrial electron transport. Curr Opin Plant Biol 2004;7:254–61.
[26] Brazhe NA, Treiman M, Brazhe AR, Find NL, Maksimov GV, Sosnovtseva OV. Mapping of redox state of mitochondrial cytochromes in live cardiomyocytes using Raman microspectroscopy. PLoS ONE 2012;7:e41990.
[27] Chen Z, Liu J, Tian L, Zhang Q, Guan Y, Chen L, et al. Raman micro-spectroscopy monitoring of cytochrome c redox state in Candida utilis during cell death under low-temperature plasma-induced oxidative stress. Analyst 2020; Online ahead of print.
[28] Zhou Y, Liu CH, Wu B, Yu X, Cheng G, Zhu K, et al. Optical biopsy identification and grading of gliomas using label-free visible resonance Raman spectroscopy. J Biomed Opt 2019;24:1–12.
[29] Jeger V, Djafarzadeh S, Jakob SM, Takala J. Mitochondrial function in sepsis. Eur J Clin Invest 2013;43:532–42.
[30] Jones AE, Shapiro NI, Trzeciak S, Arnold RC, Claremont HA, Kline JA. Lactate clearance vs central venous oxygen saturation as goals of early sepsis therapy: a randomized clinical trial. JAMA 2010;303:739–46.
[31] James JH, Luchette FA, McCarter FD, Fischer JE. Lactate is an unreliable indicator of tissue hypoxia in injury or sepsis. Lancet 1999;354:505–8.
[32] Bakker J, de Backer D, Hernandez G. Lactate-guided resuscitation saves lives: we are not sure. Intensive Care Med 2016;42:472–4.
[33] Luhr R, Cao Y, Soderquist B, Cajander S. Trends in sepsis mortality over time in randomised sepsis trials: a systematic literature review and meta-analysis of mortality in the control arm, 2002–2016. Crit Care 2019;23:241.
[34] Delano MJ, Moldawer LL. Magic bullets and surrogate biomarkers circa 2009. Crit Care Med 2009;37:1796–8.
[35] Inyushin M, Meshalkina D, Zueva L, Zayas-Santiago A. Tissue transparency in vivo. Molecules 2019;24:2388.
[36] Adar F, Erecinska M. Spectral evidence for interactions between membrane-bound hemes: resonance Raman spectra of mitochondrial cytochrome b-c1 complex as a function of redox potential. FEBS Lett 1977;80:195–200.
[37] Okada M, Smith NI, Palonpon AF, Endo H, Kawata S, Sodeoka M, et al. Label-free Raman observation of cytochrome c dynamics during apoptosis. Proc Natl Acad Sci USA 2012;109:28–32.
[38] Ash C, Dubec M, Donne K, Bashford T. Effect of wavelength and beam width on penetration in light-tissue interaction using computational methods. Lasers Med Sci 2017;32:1909–18.